

# Independent Stiffness and Force Control of Pneumatic Actuators for Contact Stability during Robot Manipulation

Xiangrong Shen

*Department of Mechanical Engineering  
Vanderbilt University  
Nashville, TN 37212, USA  
xiangrong.shen@vanderbilt.edu*

Michael Goldfarb

*Department of Mechanical Engineering  
Vanderbilt University  
Nashville, TN 37212, USA  
goldfarb@vuse.vanderbilt.edu*

**Abstract** - This paper proposes a control approach that controls the stiffness and force of pneumatic actuator independently. This independent control of stiffness and force removes a primary cause of contact instability when utilizing stiffness or impedance based force control during interaction with stiff environments. Specifically, in typical stiffness or impedance control, since the force is defined in terms of motion variables, the desired force term appears as high gain position feedback when a manipulator is in contact with a stiff environment. In the proposed approach, since stiffness and force are controlled independently, the force appears as an exogenous input rather than as high gain position feedback, and therefore this source of instability is removed. The paper describes the control approach for independent stiffness and force control, which is based on an MIMO sliding mode controller design. Experimental results are presented that demonstrate the effectiveness of the control approach.

**Index Terms** – Force control. Stiffness control. Contact stability.

## I. INTRODUCTION

A principal objective in the control of interactive robot manipulation is to impose a desired force of interaction while concurrently providing robust stability during interaction. One class of controllers theoretically well suited to maintaining stability during interaction tasks are stiffness-type and impedance-type controllers, as introduced respectively by Salisbury [1] and Hogan [2], and subsequently treated by many others. Such controllers can in theory impose a desired force on an environment, while also maintaining a passive output impedance at the robot endpoint, thus ensuring stability with a passive environment, as described by Colgate and Hogan [3]. Despite this, both control approaches can suffer from contact instability during interaction with stiff environments. Specifically, as discussed by Colgate and Hogan [3], Colgate and Hogan [4], and Eppinger and Seering [5], the ability to impose a desired passive impedance at the manipulator endpoint is significantly impaired by the fact that the force sensor is non-collocated with the actuators (i.e., the actuator, transmission, and structural dynamics of the robot manipulator are interposed between the sensor and actuator). Further, as described by An and Hollerbach [6], because the motion and force are actively coupled in

such controllers, the force sensor feedback in both approaches appears as position feedback, where the corresponding gain is largely a function of the environment stiffness. As such, contact with a stiff environment increases suddenly and drastically the position feedback gain. Since the amount of active damping imposed by a controller is limited (due to noise and phase lag in velocity measurement), the resulting dramatic increase in position gain will result in a dramatic decrease in the damping ratio of the system response, thus producing the oscillations commonly seen in contact forces with stiff environments. Further, with the added effect of non-collocation, the otherwise lightly damped, high gain system can easily become unstable. A solution to this problem, proposed by both An and Hollerbach [6] and Colgate and Hogan [4], is to utilize open-loop force control, in essence sacrificing force control accuracy for interactive stability.

This paper proposes an alternate solution to this problem that enhances the stability of interaction in closed-loop force control. Specifically, the pneumatic actuators utilized in this work enable two control degrees of freedom. One control degree of freedom is used to modulate the open-loop stiffness of the actuator, while the other is used to track a desired force. As such, the active coupling between motion and force that is inherent in standard stiffness or impedance controllers is fully eliminated. In the analysis presented by An and Hollerbach, the desired force in both stiffness and impedance controllers can be expressed in terms of motion, thus the observation that force feedback appears as high gain motion feedback. In the control approach presented herein, the desired force is an exogenous term, and as such cannot be represented as a function of the motion. The net result is that force feedback during contact with a stiff environment no longer appears as a high gain position feedback, and thus no longer destabilizes the motion dynamics of the manipulator.

## II. ACHIEVING INDEPENDENT FORCE/STIFFNESS CONTROL WITH PNEUMATIC ACTUATORS

If the opposing chambers of a pneumatic actuator can be pressurized and depressurized independently, then a desired actuation force is determined by the

difference between the respective chamber pressures, while the actuator output stiffness is affected by the weighted sum of the chamber pressures. This approach is quite similar to the manner in which humans affect motor control – differences in tension between antagonist muscle groups generates a joint torque, while the sum of the muscle tensions determines the joint stiffness. Thus, the actuator output stiffness and the actuator output force can be controlled in a nearly independent manner.

A similar approach to that proposed herein does not appear to exist in the literature. Related research includes that presented in [7], which proposed the independent control of stiffness and displacement, but their approach requires complex hardware for implementation, and experimental results indicate a limited range of stiffness control. Other related work is presented in [8], where the authors implement stiffness control of rubber-type pneumatic actuators, but utilize only a single control degree of freedom rather than two (i.e., they implement standard stiffness control in which the force and motion are actively coupled). Thus, the work does not address the contact stability issue as previously described.

This paper describes a control approach that leverages this characteristic, in order to enable stable force feedback during manipulator contact with stiff environments, as previously described. In order to obtain two control degrees of freedom for the independent control of stiffness and force, each chamber of the actuator is connected to either the compressed air supply or exhaust with a 3-way valve so that the valve opening area to each chamber of the actuator is commanded separately. Based on this configuration, a standard MIMO sliding mode approach is applied with the valve opening areas to the chambers as inputs and the stiffness and force as the outputs (i.e., each actuator is a two-input, two-output system). The controller is implemented on a single-degree-of-freedom pneumatic actuator and the performance of the controller is demonstrated with trajectory tracking at different frequencies.

### III. MODELING OF THE PNEUMATIC ACTUATOR

A typical pneumatic actuation system consists of a 4-way proportional spool valve and a pneumatic actuator, as shown in Fig. 1. In such a system, the proportional valve controls the airflow into each chamber of the actuator, thus controls the pressure differential across the piston. Since the valve opening areas to the chambers are both commanded by the 4-way valve, they are related to each other and only a single control degree of freedom is provided. To introduce an additional control degree of freedom, the 4-way valve can be decoupled into two 3-way valves, as shown in Fig. 2, hence the valve opening areas can be commanded separately.

For the actuator shown in Fig. 2, the actuation force is given by:

$$F = P_a A_a - P_b A_b - P_{atm} A_r \quad (1)$$

where  $P_a$  and  $P_b$  are the absolute pressures inside each chamber of the actuator,  $A_a$  and  $A_b$  are the effective areas of each side of the piston, and  $A_r$  is the cross-sectional area of the piston rod. In order to have the input, valve opening area  $A_v$ , to show up in the dynamics, (1) is differentiated with respect to time:

$$\dot{F} = \dot{P}_a A_a - \dot{P}_b A_b \quad (2)$$

Assuming air is an ideal gas undergoing an isothermal process, the rate of change of the pressure inside each chamber of the cylinder can be expressed as:

$$\dot{P}_{(a,b)} = \frac{RT}{V_{(a,b)}} (\dot{m}_{in(a,b)} - \dot{m}_{out(a,b)}) - \frac{P_{(a,b)}}{V_{(a,b)}} \dot{V}_{(a,b)} \quad (3)$$

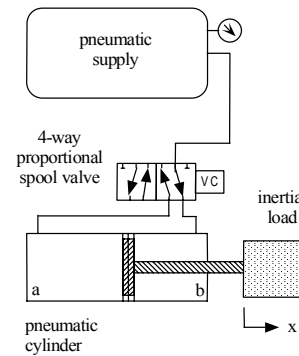


Fig. 1: Configuration of a typical pneumatic actuation system.

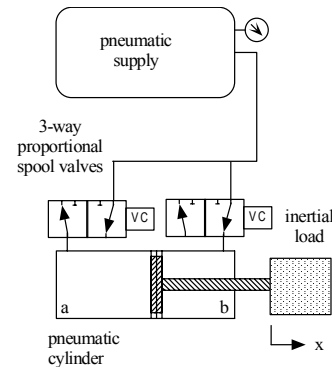


Fig. 2: Modification of the configuration to introduce an additional control DOF.

where  $P_{(a,b)}$  is the absolute pressure inside each side of the cylinder,  $\dot{m}_{in(a,b)}$  and  $\dot{m}_{out(a,b)}$  are the mass flow rates into and out of each side of the cylinder,  $R$  is the universal gas constant,  $T$  is the fluid temperature, and  $V_{(a,b)}$  is the volume of each cylinder chamber. Based on isentropic flow assumptions, the mass flow rate through a valve orifice with effective area  $A_v$  for a compressible substance will reside in either a sonic (choked) or subsonic (unchoked) flow regime:

$$\dot{m}(P_u, P_d) = \begin{cases} \sqrt{\frac{k}{RT} \left(\frac{2}{k+1}\right)^{(k+1)/(k-1)} C_f P_u A_v} & \text{if } \frac{P_d}{P_u} \leq C_r \text{ (choked)} \\ \sqrt{\frac{2k}{RT(k-1)}} \sqrt{1 - \left(\frac{P_d}{P_u}\right)^{(k-1)/k}} \left(\frac{P_d}{P_u}\right)^{1/k} C_f P_u A_v & \text{otherwise (unchoked)} \end{cases} \quad (4)$$

where  $C_f$  is the discharge coefficient of the valve,  $P_u$  and  $P_d$  are the upstream and downstream pressures, respectively,  $k$  is the ratio of specific heats,  $C_r$  is the pressure ratio that divides the flow regimes into unchoked and choked flow. The total dynamics from the valve area as input (which is an algebraic function of the spool position) to the force output is given by the combination of (2-4):

$$\dot{F} = \frac{RTA_a}{V_a} \dot{m}_a - \frac{RTA_b}{V_b} \dot{m}_b - \frac{P_a A_a}{V_a} \dot{V}_a + \frac{P_b A_b}{V_b} \dot{V}_b \quad (5)$$

where  $\dot{m}_a$  and  $\dot{m}_b$  are the net flow rates into the two chambers of the actuator, which are functions of the valve areas as expressed by (4).

#### IV. FORMULATION OF STIFFNESS OF A PNEUMATIC ACTUATOR

The output stiffness of an actuator is defined by:

$$K = -\frac{\partial F}{\partial x} \quad (6)$$

For the pneumatic actuator, the expression of actuation force  $F$  can be substituted by (1), which gives:

$$K = -\frac{\partial(P_a A_a - P_b A_b - P_{atm} A_r)}{\partial x} = -A_a \frac{\partial P_a}{\partial x} + A_b \frac{\partial P_b}{\partial x} \quad (7)$$

Assuming air is an ideal gas,

$$P_a = \frac{m_a RT}{V_a} \quad (8)$$

where  $m_a$  is the mass of air in Chamber  $a$ . And the volume in Chamber  $a$  is a function of piston displacement  $x$ :

$$V_a = A_a(x_{mid,a} + x) \quad (9)$$

where  $x_{mid,a}$  is the length of Chamber  $a$  when the displacement  $x$  is zero. Substitute (9) into (8):

$$P_a = \frac{m_a RT}{A_a(x_{mid,a} + x)} \quad (10)$$

For the calculation of the instantaneous stiffness, the air mass  $m_a$  is independent of the displacement  $x$ . Thus differentiating (10) with respect to  $x$  gives:

$$\frac{\partial P_a}{\partial x} = -\frac{m_a RT}{A_a(x_{mid,a} + x)^2} \quad (11)$$

In order to replace the air mass  $m_a$  in (11) with measurable states, substitute (10) into (11):

$$\frac{\partial P_a}{\partial x} = -\frac{P_a}{x_{mid,a} + x} \quad (12)$$

Similarly for Chamber  $b$  the pressure  $P_b$  can be expressed as

$$P_b = \frac{m_b RT}{V_b} \quad (13)$$

where  $m_b$  is the mass of air in Chamber  $b$ . And the volume in Chamber  $b$  is also a function of piston displacement  $x$ :

$$V_b = A_b(x_{mid,b} - x) \quad (14)$$

where  $x_{mid,b}$  is the length of Chamber  $b$  when the displacement  $x$  is zero. Substitute (14) into (13):

$$P_b = \frac{m_b RT}{A_b(x_{mid,b} - x)} \quad (15)$$

Differentiating (15) with respect to  $x$  gives:

$$\frac{\partial P_b}{\partial x} = \frac{m_b RT}{A_b(x_{mid,b} - x)^2} \quad (16)$$

In order to replace the air mass  $m_b$  in (16) with measurable states, substitute (15) into (16):

$$\frac{\partial P_b}{\partial x} = \frac{P_b}{x_{mid,b} - x} \quad (17)$$

Substituting (12) and (17) into (7) gives the expression of the stiffness  $K$  in the measurable state variables of the actuation system:

$$K = \frac{P_a A_a}{x_{mid,a} + x} + \frac{P_b A_b}{x_{mid,b} - x} \quad (18)$$

In order to have the inputs, the valve opening areas  $A_{v,a}$  and  $A_{v,b}$ , to show up in the dynamics, (18) is differentiated with respect to time:

$$\dot{K} = \frac{\dot{P}_a A_a}{x_{mid,a} + x} - \frac{P_a A_a \dot{x}}{(x_{mid,a} + x)^2} + \frac{\dot{P}_b A_b}{x_{mid,b} - x} + \frac{P_b A_b \dot{x}}{(x_{mid,b} - x)^2} \quad (19)$$

Substituting (3) into (19) gives

$$\dot{K} = \frac{RT}{(x_{mid,a} + x)^2} \dot{m}_a + \frac{RT}{(x_{mid,b} - x)^2} \dot{m}_b - \frac{2P_a A_a \dot{x}}{(x_{mid,a} + x)^2} + \frac{2P_b A_b \dot{x}}{(x_{mid,b} - x)^2} \quad (20)$$

(20) is the total dynamics equation from the valve areas as input (which is an algebraic function of the spool position) to the stiffness output.

#### V. MIMO SLIDING MODE CONTROLLER DESIGN

In the previous chapters the total dynamics from the valve opening area inputs to the stiffness and force outputs has been derived as (5) and (20). Thus, the standard MIMO sliding mode approach can be applied to the model for the independent control of stiffness and force as subsequently described.

For the actuation system at a certain state, the mass flow rate  $\dot{m}_a$  and  $\dot{m}_b$  are proportional to the valve

opening areas  $A_{v,a}$  and  $A_{v,b}$  respectively. Thus the mass flow rate  $\dot{m}_a$  and  $\dot{m}_b$  are taken as the inputs to the system for the convenience of controller design. Take the

input vector  $U$  as  $\begin{bmatrix} u_1 \\ u_2 \end{bmatrix} = \begin{bmatrix} \dot{m}_a \\ \dot{m}_b \end{bmatrix}$ , the output vector  $X$  as

$\begin{bmatrix} x_1 \\ x_2 \end{bmatrix} = \begin{bmatrix} F \\ K \end{bmatrix}$ , and the derivative of the output vector  $\dot{X}$

as  $\begin{bmatrix} \dot{x}_1 \\ \dot{x}_2 \end{bmatrix} = \begin{bmatrix} \dot{F} \\ \dot{K} \end{bmatrix}$ , then the dynamics (5) and (20) can be

rewritten in the matrix form as

$$\dot{X} = T + BU \quad (21)$$

where

$$T = \begin{bmatrix} t_1 \\ t_2 \end{bmatrix} \quad (22)$$

and

$$B = \begin{bmatrix} b_{11} & b_{12} \\ b_{21} & b_{22} \end{bmatrix} \quad (23)$$

The expressions for the entries of the matrices are:

$$t_1 = -\frac{P_a A_a}{V_a} \dot{V}_a + \frac{P_b A_b}{V_b} \dot{V}_b \quad (24)$$

$$t_2 = -\frac{2P_a A_a \dot{x}}{(x_{mid,a} + x)^2} + \frac{2P_b A_b \dot{x}}{(x_{mid,b} - x)^2} \quad (25)$$

$$b_{11} = \frac{RTA_a}{V_a} \quad (26)$$

$$b_{12} = -\frac{RTA_b}{V_b} \quad (27)$$

$$b_{21} = \frac{RT}{(x_{mid,a} + x)^2} \quad (28)$$

$$b_{22} = \frac{RT}{(x_{mid,b} - x)^2} \quad (29)$$

Define a sliding surface vector as

$$S = \begin{bmatrix} s_1 \\ s_2 \end{bmatrix} = \begin{bmatrix} e_1 \\ e_2 \end{bmatrix} \quad (30)$$

where  $e_1 = x_1 - x_{1d}$  and  $e_2 = x_2 - x_{2d}$ .  $x_{1d}$  and  $x_{2d}$  are the desired values of  $x_1$  and  $x_2$ , respectively. A robust control law can be developed based on a standard MIMO sliding mode approach [9] in the form of

$$U = \hat{B}^{-1}(\dot{X}_r - \hat{T} - \kappa \text{sgn}(S)) \quad (31)$$

where  $\hat{B}$  is the estimated matrix of  $B$ ,  $\hat{T}$  is the estimated vector of  $T$ ,  $\kappa$  is robustness gain vector  $\begin{bmatrix} k_1 \\ k_2 \end{bmatrix}$ ,

and  $\dot{X}_r$  is the reference input vector. By setting the time derivative of the sliding surface vector as zero, the reference input vector is derived as

$$\dot{X}_r = \begin{bmatrix} \dot{x}_{1r} \\ \dot{x}_{2r} \end{bmatrix} = \begin{bmatrix} \dot{x}_{1d} \\ \dot{x}_{2d} \end{bmatrix} \quad (32)$$

## VI. FORCE CONTROL WITH MAXIMUM/MINIMUM STIFFNESS

Control of the actuator with maximum or minimum stiffness can find many applications in robotics. With maximum stiffness, the actuator has better disturbance rejection from force to motion, while with minimum stiffness, the actuator has better disturbance rejection from motion to force. Based on the combination of the sliding mode control approach and linear optimization, a force controller can be designed with either a maximum or minimum possible output stiffness as subsequently described.

In order to drive the stiffness as high as possible, the time derivative  $\dot{K}$  should be set as the maximum value. In order to drive the stiffness as low as possible, the time derivative  $\dot{K}$  should be set as the minimum value (may be negative or positive). From the stiffness dynamics (20), it can be observed that the third and fourth terms are determined by the state of the system, while for a certain state of the actuation system the first term and second term are proportional to  $\dot{m}_a$  and  $\dot{m}_b$ , respectively. As such, the problem can be taken as an optimization problem with the object of maximizing or minimizing

$$G = b_{21}\dot{m}_a + b_{22}\dot{m}_b \quad (33)$$

where  $b_{21}$  and  $b_{22}$  are defined by (28) and (29). For the force control, the inputs should satisfy the sliding condition

$$\frac{1}{2} \frac{d}{dt} s_1^2 \leq -\eta_1 |s_1| \quad (34)$$

where  $\eta_1$  is a positive constant, and the sliding surface  $s_1$  is defined by (30). This condition can be satisfied by the following equation between the inputs:

$$b_{11}\dot{m}_a + b_{12}\dot{m}_b = -t_1 + \dot{x}_{1r} - k_1 \text{sgn}(s_1) \quad (35)$$

where  $b_{11}$  is defined by (26),  $b_{12}$  is defined by (27),  $t_1$  is defined by (24),  $\dot{x}_{1r}$  is defined by (32),  $k_1$  is the robustness gain satisfying (34), and  $s_1$  is defined by (30). Moreover, the inputs  $\dot{m}_a$  and  $\dot{m}_b$  are bounded by an upper limit for which the corresponding valve is fully open to the air supply and a lower limit for which the corresponding valve is fully open to the exhaust. These constraints can be expressed as:

$$\dot{m}_{a,\min} \leq \dot{m}_a \leq \dot{m}_{a,\max} \quad (36)$$

$$\dot{m}_{b,\min} \leq \dot{m}_b \leq \dot{m}_{b,\max} \quad (37)$$

Thus, the whole problem can be defined as maximizing or minimizing the objective function  $G$  as defined by (33) under the constraints (35), (36), and (37). The objective function and constraints are all linear, so a linear optimization approach can be applied. Fig. 3 shows the graphical method to solve this two variable problem. The constraint (35) is a straight line, while constraints (36) and (37) designate a square area. Thus, the feasible solutions are on the line segment  $AB$ . Since  $b_{11} > 0$  and  $b_{12} < 0$ , the line segment  $AB$  always has a positive tangent.

And since  $b_{21} > 0$  and  $b_{22} > 0$ , the lines of equal  $G$  always have a negative tangent. By the direction of  $G$  increasing, the maximum  $G$  can be obtained at point  $B$  while the minimum  $G$  can be obtained at point  $A$ . As such the control inputs for maximizing stiffness are

$$\dot{m}_a = \begin{cases} \dot{m}_{a,\max} & \text{when } \frac{-t_1 + \dot{x}_{1r} - k_1 \operatorname{sgn}(s_1) - b_{11}\dot{m}_{a,\max}}{b_{12}} \leq \dot{m}_{b,\max} \\ -t_1 + \dot{x}_{1r} - k_1 \operatorname{sgn}(s_1) - b_{12}\dot{m}_{b,\max} & \\ \frac{b_{11}}{b_{12}} & \\ \text{when } \frac{-t_1 + \dot{x}_{1r} - k_1 \operatorname{sgn}(s_1) - b_{11}\dot{m}_{a,\max}}{b_{12}} > \dot{m}_{b,\max} \end{cases} \quad (38)$$

$$\dot{m}_b = \begin{cases} \frac{-t_1 + \dot{x}_{1r} - k_1 \operatorname{sgn}(s_1) - b_{11}\dot{m}_{a,\max}}{b_{12}} & \text{when } \frac{-t_1 + \dot{x}_{1r} - k_1 \operatorname{sgn}(s_1) - b_{11}\dot{m}_{a,\max}}{b_{12}} \leq \dot{m}_{b,\max} \\ \dot{m}_{b,\max} & \\ \text{when } \frac{-t_1 + \dot{x}_{1r} - k_1 \operatorname{sgn}(s_1) - b_{11}\dot{m}_{a,\max}}{b_{12}} > \dot{m}_{b,\max} \end{cases} \quad (39)$$

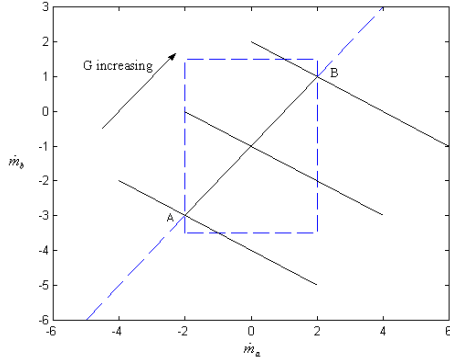


Fig. 3: Graphic method to solve the linear optimization problem.

The control inputs for minimizing stiffness are

$$\dot{m}_a = \begin{cases} \dot{m}_{a,\min} & \text{when } \frac{-t_1 + \dot{x}_{1r} - k_1 \operatorname{sgn}(s_1) - b_{11}\dot{m}_{a,\min}}{b_{12}} \geq \dot{m}_{b,\min} \\ -t_1 + \dot{x}_{1r} - k_1 \operatorname{sgn}(s_1) - b_{12}\dot{m}_{b,\min} & \\ \frac{b_{11}}{b_{12}} & \\ \text{when } \frac{-t_1 + \dot{x}_{1r} - k_1 \operatorname{sgn}(s_1) - b_{11}\dot{m}_{a,\min}}{b_{12}} < \dot{m}_{b,\min} \end{cases} \quad (40)$$

$$\dot{m}_b = \begin{cases} \frac{-t_1 + \dot{x}_{1r} - k_1 \operatorname{sgn}(s_1) - b_{11}\dot{m}_{a,\min}}{b_{12}} & \text{when } \frac{-t_1 + \dot{x}_{1r} - k_1 \operatorname{sgn}(s_1) - b_{11}\dot{m}_{a,\min}}{b_{12}} \geq \dot{m}_{b,\min} \\ \dot{m}_{b,\min} & \\ \text{when } \frac{-t_1 + \dot{x}_{1r} - k_1 \operatorname{sgn}(s_1) - b_{11}\dot{m}_{a,\min}}{b_{12}} < \dot{m}_{b,\min} \end{cases} \quad (41)$$

## VII. EXPERIMENTAL RESULTS

Experiments were conducted to validate the proposed control approach. The experimental setup, which is shown schematically in Fig. 2, incorporated a 2.7 cm (1-1/16 in) inner diameter, 10 cm (4 in) stroke pneumatic cylinder (Numatics 1062D04-04A) that was used to drive a 10 kg mass. The airflow was controlled by a pair of proportional servovalves (FESTO MPYE-5-M5-010-B), configured as three-way valves as depicted in the figure. The system was supplied with air at an absolute pressure of 653 kPa (95 psi). The model and controller parameters used in the experiments are listed in Table 1. The performance of the controller was assessed by step input responses and full-scale (i.e., range of motion of the pneumatic cylinder) sinusoidal tracking at various frequencies.

|   | Parameter          | Value | Unit            |
|---|--------------------|-------|-----------------|
| 1 | Ps                 | 653   | kPa             |
| 2 | A <sub>a</sub>     | 572   | mm <sup>2</sup> |
| 3 | A <sub>b</sub>     | 540   | mm <sup>2</sup> |
| 4 | A <sub>r</sub>     | 32    | mm <sup>2</sup> |
| 5 | A <sub>v,max</sub> | 12.57 | mm <sup>2</sup> |
| 6 | C <sub>f</sub>     | 0.8   |                 |
| 7 | M                  | 10.43 | kg              |
| 8 | B                  | 13.1  | kg*s            |
| 9 | λ                  | 20    | s <sup>-1</sup> |

Table 1: Model and controller parameters for experimental implementation.

For the force and stiffness controller, a PD control outer loop was designed to generate the desired force output for the force control. This configuration ensures highly varying chamber volumes during the force and stiffness control experiments. Fig. 4 shows the tracking performance of a commanded motion of 0.5 Hz and commanded sinusoidal stiffness variation at 0.5 Hz. Fig. 5 shows the tracking performance of a commanded motion of 2 Hz and commanded sinusoidal stiffness variation at 4 Hz. Fig. 6 shows the responses to step commands. The experimental results indicate good, independent tracking of both force and stiffness. Fig. 7 shows the force control approach with minimum stiffness, and Fig. 8 shows the corresponding results for force control with maximum stiffness.

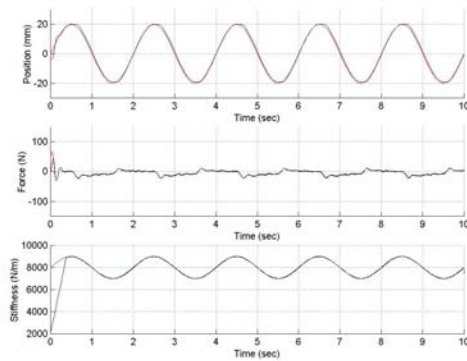


Fig. 4: Actual and desired position (outer loop), force (inner loop), and stiffness (inner loop) tracking performance of a commanded motion of 0.5 Hz and commanded sinusoidal stiffness variation of 0.5 Hz.

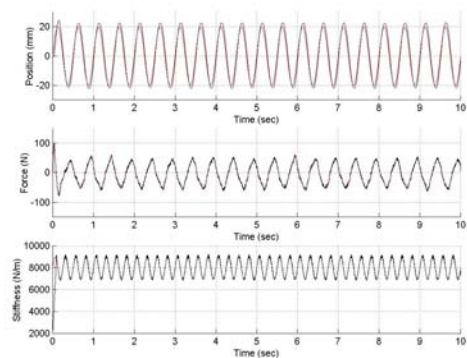


Fig. 5: Actual and desired position (outer loop), force (inner loop), and stiffness (inner loop) tracking performance of a commanded motion of 2 Hz and commanded sinusoidal stiffness variation of 4 Hz.

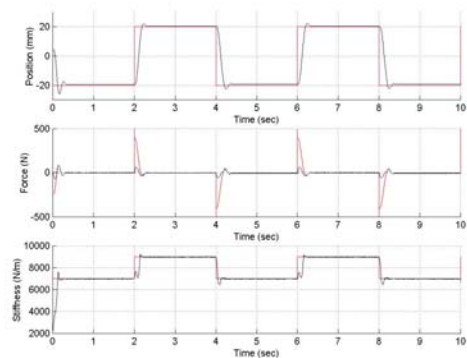


Fig. 6: Actual and desired position (outer loop), force (inner loop), and stiffness (inner loop) tracking for step commands in position and stiffness.

## VIII. CONCLUSION

The paper presented an approach capable of controlling actuator output force and stiffness independently. By successfully decoupling these quantities, the desired force term that appears as high gain position feedback in a typical stiffness control approach, appears instead in the proposed approach as an exogenous input. As such, the proposed approach holds significant promise for minimizing or eliminating contact instabilities that arise during tasks that involve

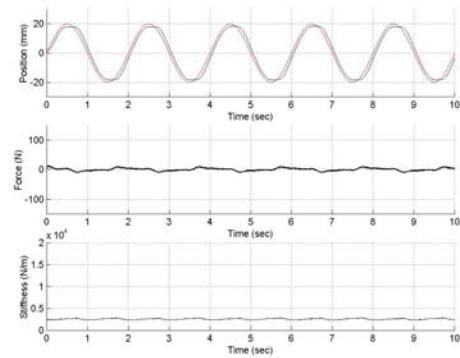


Fig. 7: Position (outer loop), force (inner loop), and stiffness (inner loop) tracking for a sinusoidal command in motion and a minimum stiffness.

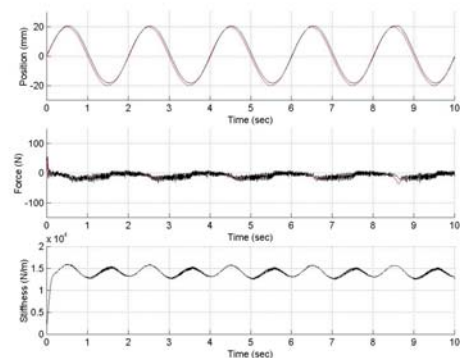


Fig. 8: Position (outer loop), force (inner loop), and stiffness (inner loop) tracking for a sinusoidal command in motion and a maximum stiffness.

closed-loop force control while in contact with a stiff environment.

## REFERENCES

- [1] Salisbury, J.K., "Active Stiffness Control of a Manipulator in Cartesian Coordinates", IEEE Conference on Decision and Control, pp. 383–388, 1980.
- [2] Hogan, N., "Impedance Control: An Approach to Manipulation", Journal of Dynamic Systems, Measurement, and Control, pp. 1–24, 1985.
- [3] Colgate, E.J., and Hogan, N., "An Analysis of Contact Instability in Terms of Passive Physical Equivalents", IEEE Conference on Robotics and Automation, pp. 404–409, 1989.
- [4] Colgate, E.J., and Hogan, N., "Robust Control of Dynamically Interacting Systems", International Journal of Control, vol. 48, no. 1, pp. 65–88, 1988.
- [5] Eppinger, S., and Seering, W., "Three Dynamic Problems in Robot Force Control", IEEE Transactions on Robotics and Automation, vol. 8, no. 6, pp. 751–758, 1992.
- [6] An, C.H., and Hollerbach, J.M., "Dynamic Stability Issues in Force Control of Manipulators", IEEE Conference on Robotics and Automation, pp. 890–896, 1987.
- [7] Koganezawa, K., and Yamazaki, M., "Mechanical Stiffness Control of Tendon-Driven Joints", IEEE/RSJ International Conference on Intelligent Robots and Systems, pp. 818–825, 1999.
- [8] Guanghua, Z., and Rong, L., "On the Implementation of Stiffness Control on a Manipulator Using Rubber Actuators", IEEE International Conference on Systems, Man and Cybernetics, pp. 183–188, 1995.
- [9] Slotine, J.E., Li, W., "Applied Nonlinear Control", Prentice Hall, NJ, 1991.